ACS APPLIED MATERIALS & INTERFACES

Research Article

www.acsami.org

Effects of pH on the Hierarchical Structures and Photocatalytic Performance of $BiVO_4$ Powders Prepared via the Microwave Hydrothermal Method

Guoqiang Tan,* Lili Zhang, Huijun Ren, Shasha Wei, Jing Huang, and Ao Xia

Key Laboratory of Auxiliary Chemistry & Technology for Chemical Industry, Ministry of Education, Shaanxi University of Science & Technology, Xi'an 710021, People's Republic of China

Supporting Information

ABSTRACT: $BiVO_4$ powders with hierarchical structures were prepared by the microwave hydrothermal method at different pHs, using $Bi(NO_3)_3{\cdot}5H_2O$ and NH_4VO_3 as raw materials. The results show that, when the pH value of the precursor is 0.59, the as-prepared powders are monoclinic $BiVO_4$ crystals with octahedron and decahedron morphologies. Spherical and polyhedral $BiVO_4$ with particle sizes in the range of 2−4 μm can be prepared under the strong acid condition (pH = 0.70−1.21) and possess a mixed crystal consisting of tetragonal and monoclinic phases, whereas rodlike and dendritic $BiVO_4$ with a pure monoclinic phase can be obtained within a very wide pH range (pH = 4.26−9.76). The phase transformation from tetragonal phase to monoclinic phase occurs at pH 3.65. At pH >9.76, the powders are the nonstoichiometric crystals between the mixed-phase $BiVO_4$ and non-$BiVO_4$. The photocatalytic efficiencies were evaluated by the degradation of Rhodamine B (RhB) under UV and simulated sunlight irradiation. The corresponding relationship among pH values of the precursor, crystalline phase, morphology, and photocatalytic performance of the powders was also discussed.

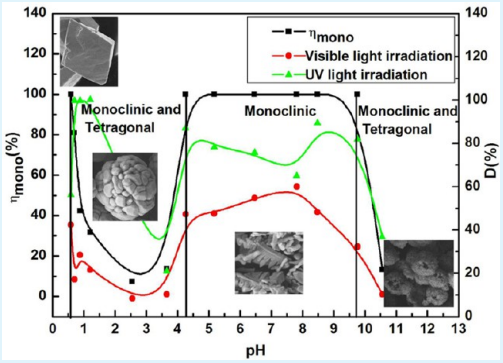

KEYWORDS: *$BiVO_4$, pH value, hierarchical structure, microwave hydrothermal method, photocatalysis*

1. INTRODUCTION

In recent years, the photocatalytic technology through semiconductors for the degradation of the organic pollutants in wastewater and air has been extensively studied.[1−3] TiO_2 has become an ideal photocatalyst, because of its nontoxicity, higher chemical stability, and oxidizability features.[4,5] However, the band gap of TiO_2 is rather wider (3.2 eV), which can only respond to the ultraviolet (UV) light covering 4% of the solar energy; this restricts the application of TiO_2.[6,7] $BiVO_4$ is a new visible-light-responsive catalyst.[8,9] Because of the narrow band gap, nontoxicity, higher stability, and higher sunlight utilization, $BiVO_4$ has drawn great attention.[10] There are three crystal structures of $BiVO_4$: a monoclinic scheelite structure (ms-$BiVO_4$), a tetragonal scheelite structure (ts-$BiVO_4$), and a tetragonal zircon structure (tz-$BiVO_4$).[11,12] Tetragonal $BiVO_4$ with a 2.9 eV band gap mainly possesses a UV absorption band, while monoclinic scheelite $BiVO_4$, with a 2.4 eV band gap, has both a visible-light absorption band and a UV absorption band. The UV bands observed in the tetragonal and monoclinic $BiVO_4$ are assigned to the band transition from O_{2p} to V_{3d}, whereas the visible light absorption is due to the transition from a valence band (VB) formed by Bi_{6s} or a hybrid orbital of Bi_{6s} and O_{2p} to a conduction band (CB) of V_{3d}.[13,14] In addition, the Bi−O bond in monoclinic $BiVO_4$ is distorted, which increases the separation efficiency of the photo-induced electrons and holes.[15,16] Then, among the three crystal types of $BiVO_4$, monoclinic $BiVO_4$ exhibits much higher photocatalytic activity than the other two tetragonal phases. Therefore, it is very important for the study on the selective preparation of monoclinic $BiVO_4$. To date, numerous methods have been employed to synthesize monoclinic $BiVO_4$ with different morphologies, such as solid-state reaction,[17] aqueous solution method,[18] co-precipitation,[1,19] solvothermal method,[20] molten salt method,[21] sonochemical method,[22] and hydrothermal method.[23,24]

It is well-known that many reaction conditions such as the precursor concentration, the nature of the surfactant, hydrothermal temperature, and time have important effects on the crystalline phase and morphology of the powders.[25] Microspheric and lamellar $BiVO_4$ powders were selectively prepared through adjustment of the hydrothermal temperature by using cetyltrimethylammonium bromide (CTAB) as a template-directing reagent.[26] Guo et al.[27] prepared $BiVO_4$ with various crystal structures and morphologies by tuning hydrothermal treatment time, acidity, and molar ratio of Bi to V in the starting materials. It is found that the pH values of the precursor solution have the great effects on the phase and morphology of $BiVO_4$ powders. With the help of triblock

Received: March 20, 2013
Accepted: May 13, 2013
Published: May 13, 2013

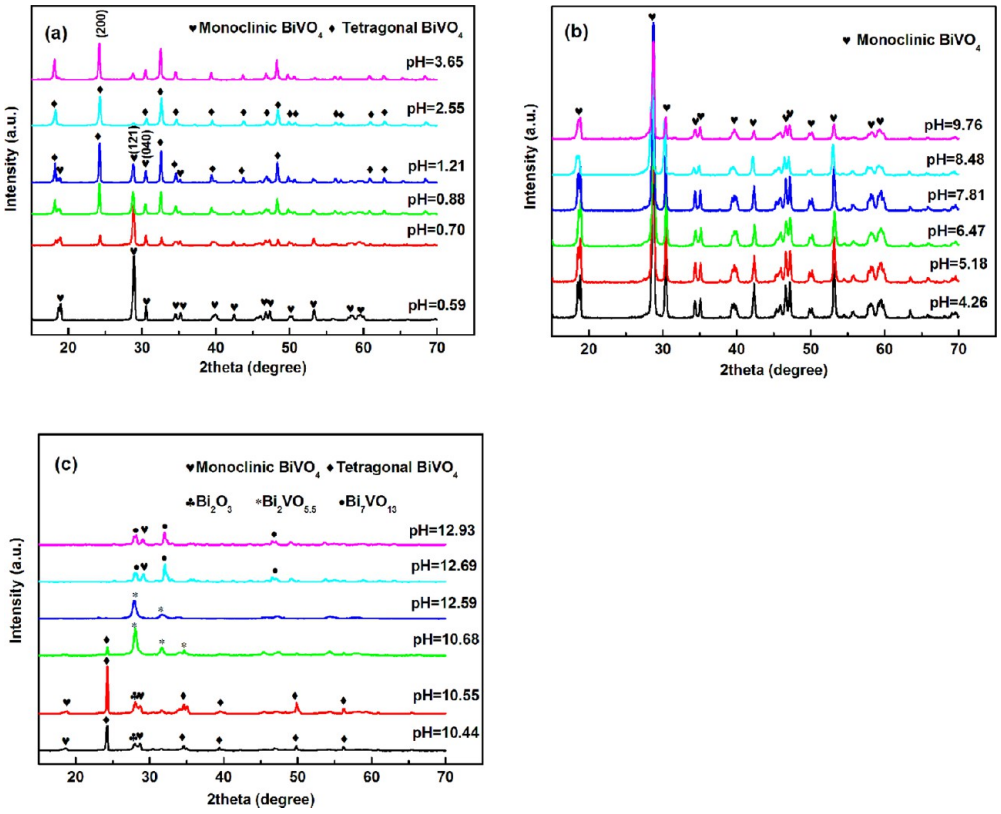

Figure 1. XRD patterns of $BiVO_4$ powders prepared by microwave hydrothermal method at different pH values: (a) pH = 0.59−3.65; (b) pH = 4.26−9.76; (c) pH = 10.44−12.93.

copolymer P123, Meng and co-workers[25] have synthesized the multi-morphology $BiVO_4$ powders by using the hydrothermal method and adjusting the pH values. They found that the rodlike $BiVO_4$ derived hydrothermally with P123 at pH 6 were able to completely degrade the Methylene Blue after 3 h of visible-light irradiation. Zhang et al.[28] studied the photocatalytic degradation of Methyl Orange over $BiVO_4$ powders prepared at different pH values. Therein, the sheetlike $BiVO_4$ prepared at pH 6.9 gave maximum photodegradation activity and the Methyl Orange was completely degraded after 1 h of visible-light irradiation. However, among these studies on the synthesis of $BiVO_4$ powders, there were few reports on the corresponding relationship among pH values of the precursor, crystalline phase, morphology, and photocatalytic performance of the powders. Herein, we reported a microwave hydrothermal route—a new quick powder synthesis method—for the selective synthesis of ms-$BiVO_4$ at different pH values and obtained the corresponding relationship among pH values of the precursor, phase, morphology, and photocatalytic performance of the powders. The possible mechanism of phase transformation at different pH conditions was also discussed.

2. EXPERIMENTAL SECTION

2.1. Photocatalyst Synthesis. All reagents were analytical-reagent (AR) grade and used without further purification. In a typical preparation, 0.01 mol $Bi(NO_3)_3{\cdot}5H_2O$ was dissolved in 20 mL distilled water and stirred for 30 min at room temperature to form a hydrolyzed white floccule suspension. A quantity of 0.01 mol NH_4VO_3 was dissolved in 20 mL of boiled distilled water and then heated and stirred for 30 min to form a transparent solution. The NH_4VO_3 solution then was added dropwise into the white floccule suspension under vigorous stirring, to form a salmon suspension. After stirring for 20 min, 5 mL of NaOH solutions with different concentrations (0−12 mol/L) were added to adjust pH values of the suspensions. After stirring for 15 min, each precursor was transferred into a 100-mL Teflon-lined stainless autoclave. The microwave hydrothermal reactions were carried out at 200 °C for 40 min in MDS-8 closed vessel microwave chemistry workstation. Finally, the precipitates were washed with distilled water and absolute ethanol three times, and then dried at 60 °C for 12 h.

2.2. Characterization Studies. The crystalline phases of the as-prepared samples were determined by X-ray diffraction (XRD) analysis (Rigaku, Model D/Max-2200). The diffraction patterns were recorded in the range of 2θ = 15°−70° using Cu Kα radiation (λ = 0.15406 nm) at a scan rate of 8° min^{-1}. The morphology and particle size of the samples were examined by field-emission scanning electron microscopy (FE-SEM) (Model JEOL, JSM-6700F). The microstructures of the samples were investigated by transmission electron microscopy (TEM) (JEOL, Model JEM-3010) and high-resolution transmission electron microscopy (HRTEM). The UV-vis absorption spectra were recorded on a UV-vis spectrophotometer (Shimadzu, Model UV-2550) in the wavelength range of 200-800 nm. $BaSO_4$ was used as the reference. The specific surface area of the samples were measured by a Brunauer−Emmett−Teller specific surface area instrument (Beishide Instrumentation Technologies (Beijing) Ltd., Model BET 3H-2000 BET-A) with nitrogen adsorption at 77 K.

2.3. Photocatalytic Activity. Photocatalytic activities of samples were determined by the decolorization of Rhodamine B (RhB) aqueous solution under simulated sunlight and UV-light irradiation. A 350-W xenon lamp was used as a simulated sunlight source and a 300 W mercury lamp was used as a UV-light source. In a typical run, 0.1 g of $BiVO_4$ was added to 50 mL of RhB solution (2×10^{-5} mol/L). Before illumination, the solutions were stirred for 30 min in darkness in order to reach the adsorption−desorption equilibrium. At given time intervals, 5 mL suspension was collected and centrifuged to remove the photocatalyst particles. The concentration of RhB was then determined by measuring the absorbance at λ_{max} = 553 nm, using a UV-vis spectrophotometer (Model SP-756p).

dx.doi.org/10.1021/am401019m | ACS Appl. Mater. Interfaces 2013, 5, 5186−5193

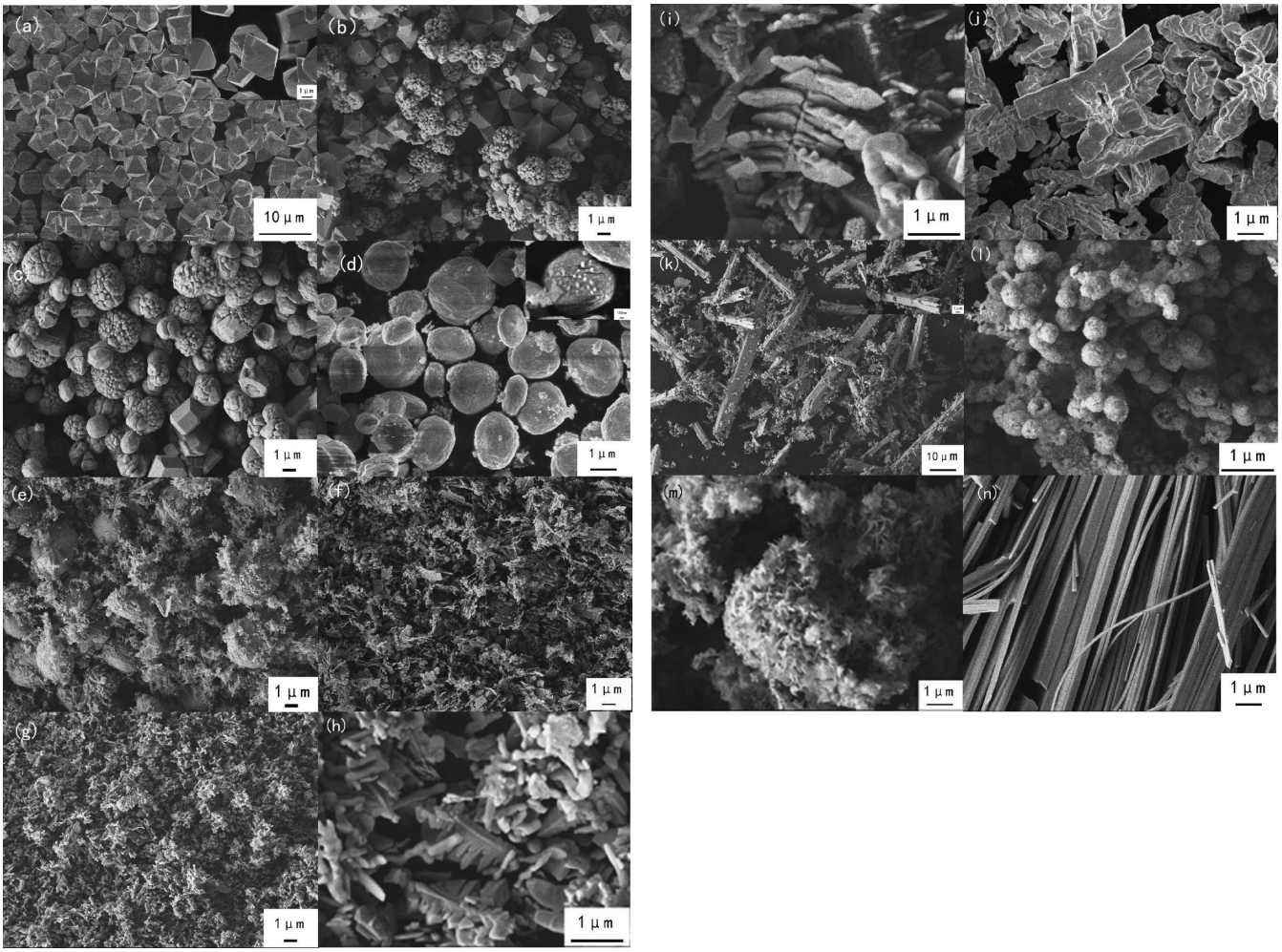

Figure 2. FESEM images of $BiVO_4$ powders prepared at different pH values: (a) 0.59, (b) 0.70, (c) 1.21, (d) 2.55, (e) 3.65, (f) 4.26, (g) 7.81, (h) 8.48, (i) 9.50, (j) 9.76, (k) 10.44, (l) 10.55, (m) 12.59, and (n) 12.93.

3. RESULTS AND DISCUSSION

3.1. XRD Analysis. Figure 1 shows XRD patterns of $BiVO_4$ powders prepared via a microwave hydrothermal method at different pH values. When the pH value of the precursor was 0.59, $Bi(NO_3)_3{\cdot}5H_2O$ was hydrolyzed (as shown by reactions 3-1 and 3-2):

$$Bi^{3+} + H_2O \leftrightarrow Bi(OH)^{2+} + H^+ \leftrightarrow Bi(OH)_2{}^+ + 2H^+ \quad (3\text{-}1)$$

$$NO_3{}^- + Bi(OH)_2{}^+ \rightarrow BiONO_3 \downarrow + H_2O \quad (3\text{-}2)$$

More H^+ species and a small amount of slightly soluble $BiONO_3$ was generated,[6,28,29] so little $BiVO_4$ was formed, as shown in reaction 3-3.

$$BiONO_3 + VO_3{}^- \rightarrow BiVO_4 \downarrow + NO_3{}^- \quad (3\text{-}3)$$

At pH $\leqslant$0.59, there were fewer crystal nuclei. Since the monoclinic sheelite $BiVO_4$ (ms-$BiVO_4$) (JCPDS No. 14-0688) was thermodynamically more stable than the polymorph with the tetragonal zircon structure (tz-$BiVO_4$) (JCPDS No. 14-0133) under strong acidic conditions (pH $\leqslant$0.59), it was easy to generate the ms-$BiVO_4$ crystals with high crystallinity.[30] However, when the pH of the precursor was suddenly increased by adding NaOH, both ms-$BiVO_4$ and tz-$BiVO_4$ could be synthesized. Since the formation of tz-$BiVO_4$ seemed to be more feasible kinetically by a sudden increase of pH, the tz-$BiVO_4$ content in the powders increased as the pH increased from 0.70 to 2.55. At pH 2.55, the amount of ms-$BiVO_4$ was decreased to the minimum. Most of the generated crystal was the tz-$BiVO_4$ (shown in Figure 1a). When the pH increased to 3.65, the diffraction peak at (121) appeared again, implying that ms-$BiVO_4$ had started to form. Once the pH increased to 4.26, pure ms-$BiVO_4$ could be obtained, as observed in Figure 1b. This was because the H^+ species was consumed gradually as the pH values constantly increased, which induced the reversible reaction equilibrium to the right direction, as shown earlier in reactions 3-1 and 3-2. Therefore, the amount of $BiONO_3$ became greater and the generated amount of $BiVO_4$ also increased. As a mineralizer, NaOH forced the generation of tz-$BiVO_4$ at the first stage and the following transformation to ms-$BiVO_4$ via a dissolution−recrystallization process.[16] From pH 4.26 to pH 9.76, with the further increase of adding content of NaOH, the mineralization of OH^- became stronger, which forced all the tz-$BiVO_4$ to transform to ms-$BiVO_4$, so the as-prepared powders were all pure ms-$BiVO_4$ powders in this pH region (as shown in Figure 1b). In addition, as a buffer, NaOH could determine the concentration of the monomer in the solution, adjust the nucleation rate and crystal growth rate of $BiVO_4$,[29] and make the crystals generate the stable monoclinic phase. The ms-$BiVO_4$ crystals first showed enhanced

Scheme 1. Summary of the Influence of Different pH Values on the Crystalline Phase and Morphology of the As-Prepared $BiVO_4$

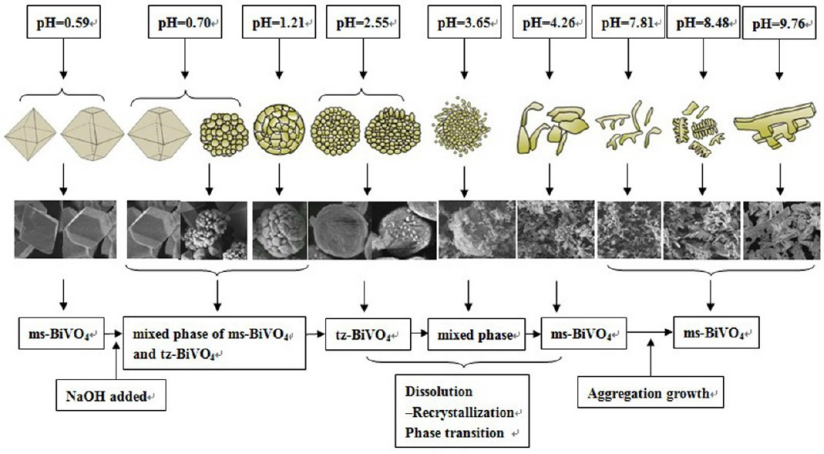

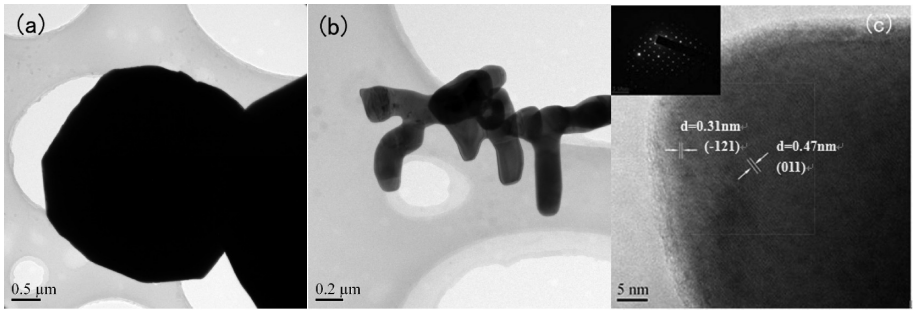

Figure 3. (a) TEM image of $BiVO_4$ powders prepared at pH 0.59; (b) TEM image and (c) HRTEM image and SAED diffraction pattern (inset) of $BiVO_4$ powders prepared at pH 7.81.

crystallinity and then a weakened tendency toward crystallization. At pH 6.47, the nucleation rate and the growth rate reached the balance. Therefore, the crystal growth was the most complete and the crystallinity was the highest. At pH 10.44, the diffraction peaks corresponding to tz-$BiVO_4$ began to appear and the intensity of the diffraction peaks was increased as the pH values increased. The as-prepared powders were mixtures of ms-$BiVO_4$ and tz-$BiVO_4$. From pH 10.55, under alkaline conditions, the Bi^{3+} species could be easily hydrolyzed and aggregated to form the high polymer (seen in reaction 3-4):

$$n\mathrm{Bi}^{3+} + 2n\mathrm{OH}^- \rightarrow [\mathrm{Bi}_n\mathrm{O}_n]^{n+} + n\mathrm{H}_2\mathrm{O} \qquad (3\text{-}4)$$

The high polymer was dissolved to generate Bi_2O_3 and $Bi_2O_{2.75}$. The following crystal phases began to appear in the powders: $Bi_2VO_{5.5}$ (JCPDS No. 51-0032), Bi_7VO_{13} (JCPDS No. 44-0322), Bi_2O_3 (JCPDS No. 74-1375), and $Bi_2O_{2.75}$ (JCPDS No. 27-0049) (see Figure 1c). On the basis of our experiment, relevant chemical reactions can be formulated as shown in reaction 3-4.

3.2. Morphology Characterization. Figure 2 shows SEM images of $BiVO_4$ powders prepared via the microwave hydrothermal method at different pH values. Scheme 1 clearly indicates the evolution process of the $BiVO_4$ crystals by varying the pH values of the precursors. At pH 0.59, the precursor substance was dissolved. When the supersaturation of the solution was increased to a relatively high value, the ms-$BiVO_4$ particles nucleate. The monomer was precipitated on the crystal nucleii and the crystals grew, which was helpful for the formation of polyhedral crystals.[31] The as-obtained $BiVO_4$ crystals possessed perfect octahedron and decahedron morphologies with sharp corners and well-defined edges. The polyhedral edge lengths were in the range of 2−3 μm, as shown in Figures 2a and Figure 3a. After adding a small amount of NaOH, a sudden increase in pH resulted in uneven nucleation, so some spherical tz-$BiVO_4$ was generated. Because the crystals grew along the different directions at different growth rates, as the reaction proceeded, the crystal plane with the higher growth rate would disappear while the crystal plane with the lower growth rate would increase in area. Since the growth rate of the (121) facets was greater than that of the (040) facets, the area of the (121) facets became smaller while the area of the (040) facets became larger, resulting in the disappearance of the apexes of octahedron crystals, as shown in Figure 2b. The intensity ratios of (121)/(040) increased as the pH increased (see Figure S1 in the Supporting Information). This result is consistent with the SEM analysis. At pH 1.21, the as-produced powders had two types of morphologies. One was the dense decahedron and irregular polyhedron caused by the dissolution of octahedral edges (Figure 2c). The other was a loose sphere composed of the small polyhedron crystals. The formation of the crystal seeds consumed more intermediate products. Thus, the amount of the monomer precipitated on every crystal seed was decreased. The bigger nucleation rate and the smaller crystal growth rate resulted in the space between small crystals. As the pH increased to 2.55, more monomers were generated and then aggregated on the seed. Every small grain grew further and was piled together densely to become the dense sphere with a diameter of 2−3 μm or an oblate spheroid 1 μm in

dx.doi.org/10.1021/am401019m | ACS Appl. Mater. Interfaces 2013, 5, 5186−5193

diameter (Figure 2d). The small amount of nanoparticles were scattered around the sphere, as shown in the inset of Figure 2d. When the pH was increased to 3.65, NaOH played its strong mineralization ability. Phase transformation from the tetragonal phase to the monoclinic one took place during the recrystallization process.[30] The tz-$BiVO_4$ crystals were dissolved and recrystallized to ms-$BiVO_4$. The monoclinic small grains began to escape from the tetragonal spherical crystals (seen in Figure 2e). The small grains composed of the sphere grew from the surface and escaped from the surface. They were then connected with other grains to grow into irregular dendritic crystals, and the sizes of the crystals were about dozens of nanometers. At pH 4.26, the tetragonal spherical-shaped crystals disappeared completely and were transformed to the monoclinic irregular sheetlike and short rodlike crystals (Figure 2f). At pH 7.81, the nucleation rate of the crystal was smaller than the growth rate. The generated crystals were all irregular rodlike or dendritic crystals with dimensions of ~100 nm (Figure 2g). It can be seen from the TEM image (Figure 3b) that the crystal was three short rods 0.20 μm in diameter, growing from the long rod with a diameter of 0.23 μm. From the inset in Figure 3c, the SAED diffraction patterns were the bright spots of electron diffraction, which indicated that the as-prepared $BiVO_4$ was single crystalline. The clear lattice fringe indicated the high crystallinity. The *d*-spacings were measured to be 0.31 and 0.47 nm, which agreed well with the lattice spacings of $(\bar{1}21)$ and (011) of ms-$BiVO_4$. At pH 8.48, the crystals grew further. A large amount of irregular long-rod-like crystals and a small amount of fish-rib-like crystals with the trunk length of 1 μm and a branch length of hundreds of nanometers appeared (seen in Figure 2h). At pH 9.50, the short-rod-like crystal grains gradually dissolved and recrystallized. The grains were transformed from the small-size grain surface to the large-size grain surface. The long-rod-like crystals were changed to sheetlike crystals. Both the trunk and branch of the fish-rib-like crystals grew bigger and the crystal surface became rough (Figure 2i). At pH 9.76, the crystals grew to be several micrometers, the morphology was irregular and the aggregation was serious. There were some fish-rib-like crystals with a trunk length of ~5 μm and the branch length of ~1 μm (Figure 2j). At pH 10.44, the hollow tubular crystals 20–50 μm in length were generated. The cross section of the hollow tube was square (Figure 2k), and the side length of the square was ~1–2 μm. From the inset of Figure 2k, it could be seen that the hollow tube was composed of many long rods with a side length of 300 nm. On the surface and the surroundings of the hollow tube were scattered small spheres 300 nm in diameter. At pH 10.55, the powders were hollow spheres 0.5–0.6 μm in diameter. The hollow sphere was composed of many smaller grains. Some individual hollow spheres were not completely closed (Figure 2l). At pH 12.59, the powders were formed by the aggregation of the sheetlike substance hundreds of nanometers in size (Figure 2m). When the pH was 12.93, the bandlike substance hundreds of nanometers in width and ~10 μm in length was formed, and its surface was smooth (Figure 2n).

The XRD, FESEM, and TEM results suggest that the pH values of the precursors affect not only the crystal structure, but also the morphology of as-prepared $BiVO_4$; moreover, for ms-$BiVO_4$, different morphologies can be selectively synthesized by adjusting the pH values of the precursors.

3.3. UV-Vis Absorption Spectra Analysis. The diffuse reflectance spectra of the prepared $BiVO_4$ samples are shown in Figure 4. All the samples showed very strong absorption in the UV-light region, while, in the visible light region, the absorption

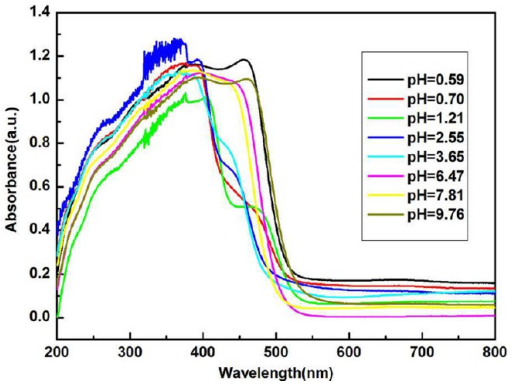

Figure 4. UV-vis diffuse reflectance absorption spectra of $BiVO_4$ powders prepared via the microwave hydrothermal method at different pH values.

intensity was obviously different. The powders prepared at pH = 0.70–3.65 showed weak absorption in the visible-light regions (400–500 nm). At pH 1.21, the absorption curve of the as-prepared powders showed the apparent step-like within regions of 420–500 nm, which was related to its mixed-phase structure. The monoclinic powders prepared at pH 0.59 and in the pH region of 6.47–9.76 still possessed strong absorption in the visible-light regions. The spectra were steep, which indicated that the visible-light absorption was not due to the transition from the impurity level but, rather, the band-gap transition.[10,32] The band gaps estimated by extrapolating the linear region of a plot of the absorbance squared vs energy[33] are 2.40, 2.43, 2.48, and 2.33 eV for ms-$BiVO_4$ (pH 0.59), ms-$BiVO_4$ (pH 6.47), ms-$BiVO_4$ (pH 7.81), and ms-$BiVO_4$ (pH 9.76), respectively. These results were similar to the previous reports[34,35] and indicated the electronic structure of $BiVO_4$ was changed as the crystalline phase changed.

3.4. Photocatalytic Activity for Rhodamine B (RhB) Degradation. The photocatalytic activities of the $BiVO_4$ prepared at different pH values were evaluated through RhB degradation under UV light and simulated sunlight. Figure 5 displayed the temporal evolution of the spectral changes during the photodegradation of RhB over $BiVO_4$ (pH 1.21) under UV-light illumination. From the spectra, it could be seen that, with the prolongation of the irradiation time, the absorbance of RhB

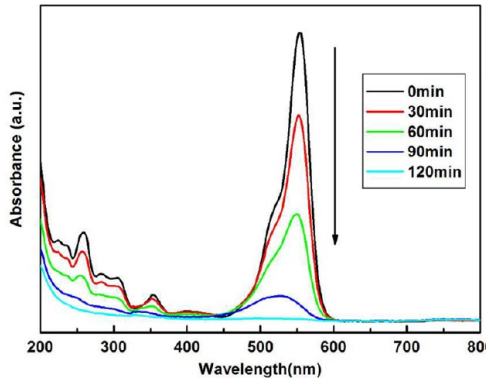

Figure 5. Time-dependent UV-vis absorption spectra of the RhB solution in the presence of $BiVO_4$ powders prepared at pH 1.21.

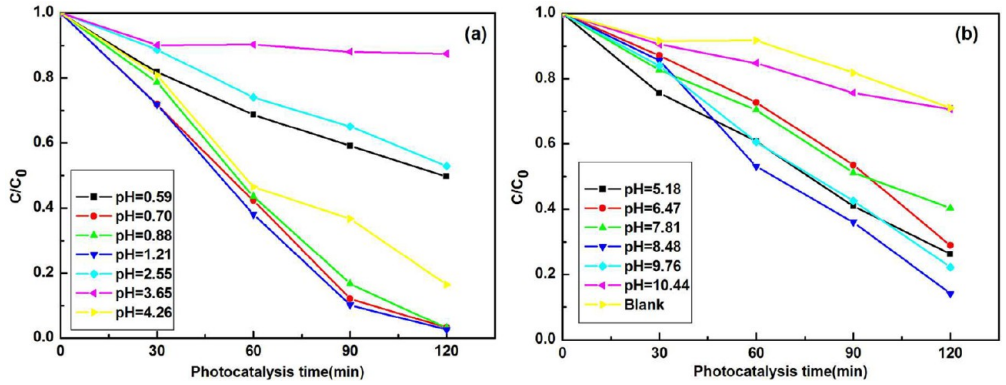

Figure 6. Photocatalytic degradation ratio of RhB versus UV-light irradiation time, using various photocatalysts.

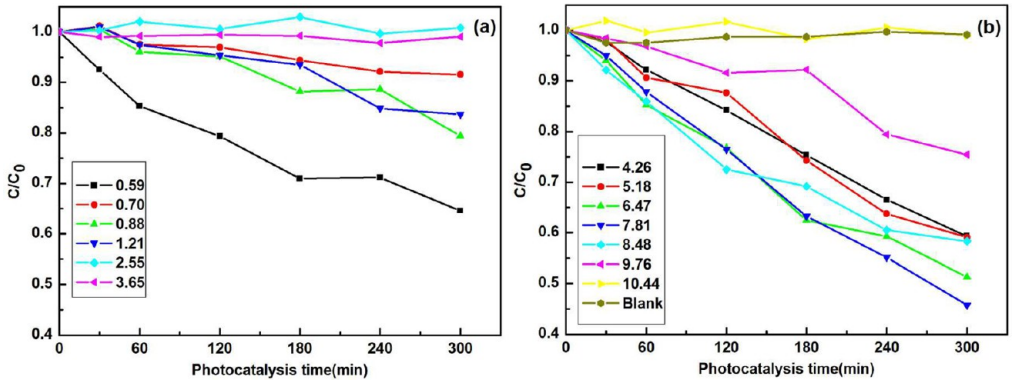

Figure 7. Photocatalytic degradation ratio of RhB versus simulated sunlight irradiation time, using various photocatalysts.

at the maximum absorption wavelength (553 nm) was gradually decreased, which was because the chromophoric structure of the dye was destroyed. In addition, the major absorption band shifts from 553 nm to 495 nm, indicating the de-ethylation of RhB molecules.[30] After 2 h of UV-light irradiation, the degradation rate of RhB solution could reach 97%, indicating that most of the RhB has been degraded.

Figure 6 showed the photocatalytic performance (C/C_0) versus UV-light irradiation time of the as-fabricated $BiVO_4$ powders for RhB degradation in an aqueous solution. For comparison, direct photolysis of dye solution was performed under the same conditions without photocatalysts. According to the degradation rate of RhB, within 2 h of UV-light irradiation, it could be seen that the catalytic activity order of the different photocatalysts was as follows: $BiVO_4$ (pH 0.70, 1.21, 0.88, mixed phase) > $BiVO_4$ (pH 0.59, 4.26, 5.18, 6.47, 7.81, 8.48, 9.76, monoclinic phase) > $BiVO_4$ (pH 2.55, tetragonal phase) > $BiVO_4$ (pH 3.65, 10.44, mixed phase). Three mixed-phase-structure powders (pH 0.70, 1.21, 0.88) exhibited the highest UV-light photocatalytic activity among all samples, and the degradation rates of the powders, relative to the RhB solution, were all >97%. Under the same conditions, the ms-$BiVO_4$ showed lower UV-light activity, compared to the mixed-phase $BiVO_4$ (pH 0.70, 1.21, 0.88), and more than 50% of the RhB could be degraded. However, the photocatalytic efficiency of tz-$BiVO_4$ (pH 2.55) and mixed-phase structure powders (pH 3.65, 10.44) was obviously lower than that of other samples. Many studies have proved that the photocatalytic activity of $BiVO_4$ have a close relationship to the crystal structure.[36,37] Our study found that the mixed-phase $BiVO_4$ (pH 0.70, 1.21, 0.88) showed higher photocatalytic efficiency under UV light than that of ms-$BiVO_4$, tz-$BiVO_4$, and mixed-phase-structure powders (pH 3.65, 10.44). This was because $BiVO_4$ co-existing with two different crystal structures was similar to the semi-conductor coupling. For tz-$BiVO_4$, with a band-gap energy of 2.9 eV,[6] its valence band (VB) and conduction band (CB) were formed by O_{2p} and V_{3d} orbits, respectively. As for ms-$BiVO_4$, its CB was formed by V_{3d} orbits and its VB was composed of not only O_{2p} but also Bi_{6s} (namely, a hybrid orbital of O_{2p} and Bi_{6s}). The presence of Bi_{6s} in the top of the VB resulted in a more-negative energy level of the VB and then a decrease in the band gap.[26] Under the UV-light irradiation, the electrons in the VBs of tz-$BiVO_4$ and ms-$BiVO_4$ could be excited to their conduction bands. The difference of band position between tz-$BiVO_4$ and ms-$BiVO_4$[38] increased the separating efficiency of the electrons and holes, to prolong the lifespan of the electrons and holes and to restrict the recombination of the charge carriers. However, the amount of tz-$BiVO_4$ in mixed-phase powders was critical for the performance. Since the photocatalytic activity of tz-$BiVO_4$ was lower than that of ms-$BiVO_4$, too much tz-$BiVO_4$ existing in the mixed-phase powders would result in a decrease in photocatalytic efficiency. This was the main reason for the tz-$BiVO_4$ and mixed-phase-structure powders (pH 3.65, 10.44) exhibited lower photocatalytic efficiency than other samples. In addition, much research has shown that the surface area of a photocatalyst is an important factor that influences its photocatalytic performance.[32,39]As can be seen from Table S1 in the Supporting Information, although the mixed phase $BiVO_4$ (pH 0.70, 1.21, 0.88) possessed much lower surface areas (0.54−0.91 m^2/g) than other samples, except for ms-$BiVO_4$ (pH 0.59), they exhibited much higher photocatalytic

dx.doi.org/10.1021/am401019m | ACS Appl. Mater. Interfaces 2013, 5, 5186−5193

activities than others. These results indicated that the surface area did not significantly influence the activities of the $BiVO_4$ samples under UV-light irradiation.

Figure 7 shows degradation rate−time curves of RhB solution with $BiVO_4$ powders as catalysts under simulated sunlight irradiation. Based on the degradation rate of RhB within 5 h simulated sunlight irradiation, the catalytic activity order of the various catalyst samples could be obtained as follows: $BiVO_4$ (pH 0.59, 4.26, 5.18, 6.47, 7.81, 8.48, 9.76, monoclinic phase) > $BiVO_4$ (pH 0.70, 0.88, 1.21, 3.65, 10.44, mixed phase) > $BiVO_4$ (pH 2.55, tetragonal phase). As mentioned in the Introduction, tz-$BiVO_4$ with a 2.9 eV band gap mainly possessed a UV absorption band, while ms-$BiVO_4$ with a 2.4 eV band gap had both a visible-light absorption band and a UV absorption band.[13] Under the simulated sunlight irradiation, ms-$BiVO_4$ could absorb visible light and generate photoelectrons and holes to participate the oxidation−reduction reaction. However, the photocatalytic process over tz-$BiVO_4$ could only be activated by UV light, which was less in the simulated sunlight, so the photocatalysis of tz-$BiVO_4$ could be negligible.[16] As a result, the degradation rates of RhB decreased as the tz-$BiVO_4$ content increased under the simulated sunlight irradiation. In addition, although the prepared powders were all ms-$BiVO_4$ powders at pH 0.59 and in the pH range of 4.26−9.76, respectively, their photocatalysis activities under simulated sunlight were very different, which was due to the differences of their special morphologies and the specific surface areas. At pH 9.76, the aggregation of the bigger size crystals was very serious. The specific surface area of the powders was estimated to be 1.29 m^2/g, as shown in Table S1 in the Supporting Information. At pH 0.59, the grain size of the prepared powders was bigger and the surface was smooth. The specific surface area of the powders was only 0.16 m^2/g. At pH = 4.26−7.81, the crystals showed irregular rodlike or dendritic morphologies. The size of the crystal particles was much smaller than others. The specific surface area of the powders were in the range of 4.20−5.76 m^2/g, which were much higher than those of ms-$BiVO_4$ (pH 0.59) and ms-$BiVO_4$ (pH 9.76). These results revealed that, under simulated sunlight irradiation, the photocatalytic activity of ms-$BiVO_4$ was not only related to the crystal types, but greatly to its morphology, size, and specific surface area.

Figure 8 was the relationship between the hierarchical structures and photocatalytic performance of $BiVO_4$ prepared via the microwave hydrothermal method in different pH regions. The amount of the ms-$BiVO_4$ was calculated by

$$\eta_{mono} = \frac{I_{mono(121)}}{I_{mono(121)} + I_{tetra(200)}}$$

among which η_{mono}, $I_{mono(121)}$, and $I_{tetra(200)}$ represented the amount of the monoclinic phase, the relative intensity of (121) diffraction peak for the monoclinic phase, and that of the (200) peak for the tetragonal phase, respectively.[40] At pH ≤0.59 in the precursor solution, η_{mono} = 100%. The powders were all ms-$BiVO_4$. The degradation rate of RhB after 2 h of UV-light irradiation was 50%. The degradation rate of RhB after 5 h of simulated sunlight irradiation was 35%. Within pH = 0.59−2.55, the amount of ms-$BiVO_4$ was gradually decreased as the pH values increased, but the trend of the photocatalytic activities under UV-light irradiation differs from that under simulated sunlight irradiation. Under simulated sunlight irradiation, the degradation rates of RhB were directly proportional to the amount of ms-$BiVO_4$. Under UV-light irradiation, the mixed phase $BiVO_4$ (pH 0.70, 1.21, 0.88) (η_{mono} = 31.64%−80.89%) showed much higher photocatalytic activities than that of tz-$BiVO_4$ and mixed-phase-structure powders (pH 3.65, 10.44) (η_{mono} = 13.59%, 13.28%). At pH = 4.26−9.76, the as-prepared powders were all ms-$BiVO_4$. At pH 7.81, the as-prepared powder showed the best photocatalytic activity under the simulated sunlight irradiation in this work. The degradation rate of RhB after 5 h of simulated sunlight irradiation was 54%. At pH ≥9.76, the amount of ms-$BiVO_4$ was obviously decreased and then the photocatalytic activity also was decreased.

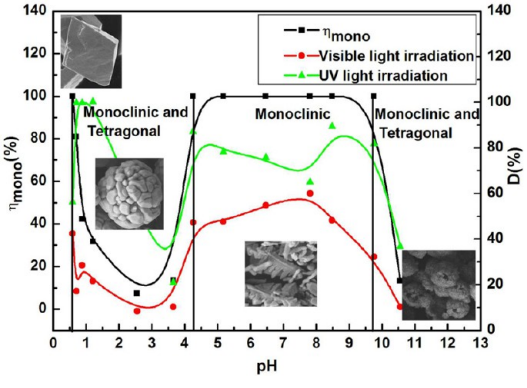

Figure 8. Relationship between the hierarchical structures and photocatalytic performance of $BiVO_4$ prepared in different pH regions.

4. CONCLUSION

In summary, $BiVO_4$ powders with the hierarchical structures have been prepared via the microwave hydrothermal method, and their photocatalytic activities were investigated. It is found that the $BiVO_4$ with different crystal phases and morphologies can be prepared by varying the pH values of the precursors. The octahedron and decahedron monoclinic scheelite structure (ms-$BiVO_4$) can be synthesized at pH 0.59. Spherical and polyhedral $BiVO_4$ possessing a mixed phase of tetragonal and monoclinic phases can be prepared at pH = 0.70−1.21, which was able to completely degrade the Rhodamine B (RhB) after 2 h of UV-light irradiation. At pH 2.55, the tetragonal zircon structure (tz-$BiVO_4$) crystals with a ball morphology are obtained. At pH 3.65, the tetragonal phase is transformed to the monoclinic phase and the dendritic monoclinic crystal dozens of nanometers in size appears. At pH = 4.26−9.76, the synthesized $BiVO_4$ powders are pure monoclinic phase. The crystal morphology is irregular rodlike or dendritic and finally evolves into a fish-rib-like structure. At pH 7.81, the ms-$BiVO_4$ with high specific surface area (5.16 m^2/g) exhibits the best visible-light photocatalytic activity, indicating that visible-light photocatalytic activity of $BiVO_4$ is not only related to the crystal structure, but greatly to its morphology and specific surface area. At pH >9.76, the prepared powders are the mixed phase $BiVO_4$, and $Bi_2VO_{5.5}$, Bi_7VO_{13}, Bi_2O_3, and $Bi_2O_{2.75}$ crystal phases. The photocatalytic activities of the powders begin to decrease.

dx.doi.org/10.1021/am401019m | ACS Appl. Mater. Interfaces 2013, 5, 5186−5193

■ ASSOCIATED CONTENT

Supporting Information

The correlations of the pH with the intensity ratios of (121)/(040) in the XRD patterns of the corresponding $BiVO_4$ samples and BET surface areas of the as-prepared $BiVO_4$ samples. This material is available free of charge via the Internet at http://pubs.acs.org.

■ AUTHOR INFORMATION

Corresponding Author

*E-mail address: tan3114@163.com.

Notes

The authors declare no competing financial interest.

■ ACKNOWLEDGMENTS

This work is supported by the Project of the National Natural Science Foundation of China (Grant No. 51172135); State-Level College Students' Innovation and Entrepreneurship Training Program for Local Colleges and Universities (No. 201210708022); the Graduate Innovation Fund of Shaanxi University of Science and Technology (No. SUST-A04); Green Manufacturing of Ceramic Materials with Novel Functional Application Innovation Team Assistance Fund of Shaanxi University of Science and Technology (No. TD12-05).

■ REFERENCES

(1) Fan, H. M.; Jiang, T. F.; Li, H. Y.; Wang, D. J.; Wang, L. L.; Zhai, J. L.; He, D. Q.; Wang, P.; Xie, T. F. *J. Phys. Chem. C* **2011**, *116*, 2425−2430.
(2) Saison, T.; Chemin, N.; Chanéac, C.; Durupthy, O.; Ruaux, V.; Mariey, L.; Maugé, F.; Beaunier, P.; Jolivet, J.-P. *J. Phys. Chem. C* **2011**, *115*, 5657−5666.
(3) Fu, Y.; Sun, X.; Wang, X. *Mater. Chem. Phys.* **2011**, *131*, 325−330.
(4) Sun, S.; Wang, W.; Zeng, S.; Shang, M.; Zhang, L. *J. Hazard. Mater.* **2010**, *178*, 427−433.
(5) Rehman, S.; Ullah, R.; Butt, A. M.; Gohar, N. D. *J. Hazard. Mater.* **2009**, *170*, 560−569.
(6) Yin, W.; Wang, W.; Zhou, L.; Sun, S.; Zhang, L. *J. Hazard. Mater.* **2010**, *173*, 194−199.
(7) Wetchakun, N.; Chaiwichain, S.; Inceesungvorn, B.; Pingmuang, K.; Phanichphant, S.; Minett, A. I.; Chen, J. *ACS Appl. Mater. Interfaces* **2012**, *4*, 3718−3723.
(8) Luo, H. M.; Mueller, A. H.; McCleskey, T. M.; Burrell, A. K.; Bauer, E.; Jia, Q. X. *J. Phys. Chem. C* **2008**, *112*, 6099−6102.
(9) Kho, Y. K.; Teoh, W. Y.; Iwase, A.; Mädler, L.; Kudo, A.; Amal, R. *ACS Appl. Mater. Interfaces* **2011**, *3*, 1997−2004.
(10) Dunkle, S. S.; Helmich, R. J.; Suslick, K. S. *J. Phys. Chem. C* **2009**, *113*, 11980−11983.
(11) Zhang, L.; Chen, D. R.; Jiao, X. L. *J. Phys. Chem. B* **2006**, *110*, 2668−2673.
(12) Zhang, A. P.; Zhang, J. Z. *Mater. Lett.* **2009**, *63*, 1939−1942.
(13) Kudo, A.; Omori, K.; Kato, H. *J. Am. Chem. Soc.* **1999**, *121*, 11459−11467.
(14) Ng, Y. H.; Iwase, A.; Kudo, A.; Amal, R. *J. Mater. Sci. Lett.* **2010**, *1*, 2607−2612.
(15) Wang, W. Z.; Shang, M.; Yin, W. Z.; Ren, J.; Zhou, L. *J. Inorg. Mater.* **2011**, *27*, 11−18.
(16) Tokunaga, S.; Kato, H.; Kudo, A. *Chem. Mater.* **2001**, *13*, 4624−4628.
(17) Kudo, A.; Ueda, K.; Kato, H.; Mikami, I. *Catal. Lett.* **1998**, *53*, 229−230.
(18) Zhou, L.; Wang, W. Z.; Xu, H. L. *Cryst. Growth Des.* **2008**, *8*, 728−733.
(19) Ke, D. N.; Peng, T. Y.; Ma, L.; Cai, P.; Jiang, P. *Appl. Catal., A* **2008**, *350*, 111−117.
(20) Ren, L.; Jin, L.; Wang, J. B.; Yang, F.; Qiu, Mi. Q.; Yu, Y. *Nanotechnology* **2009**, *20*, 115603.
(21) Liu, Y.; Ma, J.; Liu, Z.; Dai, C.; Song, Z.; Sun, Y.; Fang, J.; Zhao, J. *Ceram. Int.* **2010**, *36*, 2073−2077.
(22) Zhou, L.; Wang, W. Z.; Liu, S.; Zhang, L.; Xu, H.; Zhu, W. *J. Mol. Catal. A: Chem.* **2006**, *252*, 120−124.
(23) Zhou, Y.; Vuille, K.; Heel, A.; Probst, B.; Kontic, R.; Patzke, G. R. *Appl. Catal., A* **2010**, *375*, 140−148.
(24) Zhang, A. P.; Zhang, J. Z. *Appl. Surf. Sci.* **2010**, *256*, 3224−3227.
(25) Meng, X.; Zhang, L.; Dai, H.; Zhao, Z.; Zhang, R.; Liu, Y. *Mater. Chem. Phys.* **2011**, *125*, 59−65.
(26) Ke, D. N.; Peng, T. Y.; Ma, L.; Cai, P.; Dai, K. *Inorg. Chem.* **2009**, *48*, 4685−4691.
(27) Guo, Y.; Yang, X.; Ma, F.; Li, K.; Xu, L.; Yuan, X. *Appl. Surf. Sci.* **2010**, *256*, 2215−2222.
(28) Zhang, A. P.; Zhang, J. Z.; Cui, N. Y.; Tie, X. Y.; An, Y. W.; Li, L. *J. Mol. Catal. A: Chem.* **2009**, *304*, 28−32.
(29) Madhusudan, P.; Ran, J. R.; Zhang, J.; Yu, J. G.; Liu, G. *Appl. Catal., B* **2011**, *110*, 286−295.
(30) Zhou, L.; Wang, W. Z.; Zhang, L. S.; Xu, H. L.; Zhu, W. *J. Phys. Chem. C* **2007**, *111*, 13659−13664.
(31) Sui, Y. M.; Fu, W. Y.; Yang, H. B.; Zeng, Y.; Zhang, Y. Y.; Zhao, Q.; Li, Y. G.; Zhou, X. M.; Leng, Y.; Li, M. H.; Zou, G. T. *Cryst. Growth Des.* **2010**, *10*, 99−108.
(32) Li, G. S.; Zhang, D. Q.; Yu, J. C. *Chem. Mater.* **2008**, *20*, 3983−3992.
(33) Cao, S. W.; Yin, Z.; Barber, J.; Boey, F. Y. C.; Loo, S. C. J.; Xue, C. *ACS Appl. Mater. Interfaces* **2011**, *4*, 418−423.
(34) Sun, S. M.; Wang, W. Z.; Zhou, L.; Xu, H. L. *Ind. Eng. Chem. Res.* **2009**, *48*, 1735−1739.
(35) Jiang, H. Y.; Meng, X.; Dai, H. X.; Deng, J. G.; Liu, Y. X.; Zhang, L.; Zhao, Z. X.; Zhang, R. Z. *J. Hazard. Mater.* **2012**, *217-218*, 92−99.
(36) Zhang, A. P.; Zhang, J. Z. *J. Alloys Compd.* **2010**, *491*, 631−635.
(37) Wang, F. X.; Shao, M. W.; Cheng, L.; Hua, J.; Wei, X. W. *Mater. Res. Bull.* **2009**, *44*, 1687−1691.
(38) Stoltzfus, M. W.; Woodward, P. M.; Seshadri, R.; Klepeis, J. H.; Bursten, B. *Inorg. Chem.* **2007**, *46*, 3839−3850.
(39) Guan, M. L.; Ma, D. K.; Hu, S. W.; Chen, Y. J.; Huang, S. M. *Inorg. Chem.* **2010**, *50*, 800−805.
(40) Bhattacharya, A. K.; Mallick, K. K.; Hartridge, A. *Mater. Lett.* **1997**, *30*, 7−13.